Available online at www.sciencedirect.com
SCIENCE DIRECT®
Catalysis Today 98 (2004) 505–509
CATALYSIS TODAY
www.elsevier.com/locate/cattod

Photocatalytic conversion of CH_4 and CO_2 to oxygenated compounds over Cu/CdS–TiO_2/SiO_2 catalyst

Daxin Shi, Yaqing Feng, Shunhe Zhong*

School of Chemical Engineering and Technology, Tianjin University, Tianjin 300072, China

Abstract

Coupled semiconductor (CS) Cu/CdS–TiO_2/SiO_2 photocatalyst was prepared using a mutli-step impregnation method. Its optical property was characterized by UV–vis spectra. BET, XRD, Raman and IR were used to study the structure of the photocatalyst. Fine CdS was found dispersed over the surface of anatase TiO_2/SiO_2 substrate. Chemisorption and IR analysis showed methane absorbed in the molecular state interacted weakly with the surface of catalyst, and the interaction of CO_2 with CS produced various forms of absorbed CO_2 species that were primarily present in the form of formate, bidentate and linear absorption species. Photocatalytic direct conversion of CH_4 and CO_2 was performed under the operation conditions: 373 K, 1:1 of CO_2/CH_4, 1 atm, space velocity of 200 h^{-1} and UV intensity of 20.0 mW/cm^2. The conversion was 1.47% for CH_4 and 0.74% for CO_2 with a selectivity of acetone up to 92.3%. The reaction mechanisms were proposed based on the experimental observations.

Keywords: CH_4; CO_2; Acetone; Photocatalysis; Mechanism

1. Introduction

Conversion and utilization of CO_2 as well as CH_4 are important subjects in the field of C_1 chemistry. Converting CO_2 is desirable because of its adverse greenhouse effect. CH_4, the principal component of natural gas, is one of the most abundant, low-cost, carbon-based feedstock. Therefore, direct conversion of CO_2 and CH_4 to oxygenated compound is very attractive. However, there is no practical technique for such conversion. Direct synthesis of oxygenated compounds from CO_2 and CH_4 has been studied in only a few cases [1–5]. Fujiwara et al. [1] reported that high yields of acetic acid resulted from the direct reaction of CH_4 with CO_2 by means of homogeneous catalysis at 80 °C using a $Pd(OAc)_2$/$Cu(OAc)_2$/$K_2S_2O_8$/TFA catalyst. Huang et al. [2] investigated the direct conversion of CO_2 and CH_4 by means of a two-step method and observed the formation of alcohol, aldehyde, ketone, carboxylic acid, and cyclopentane derivatives. Liu et al. [3] used a method of dielectric-barrier discharge plasma for methane conversion in the presence of CO_2, with which oxygenates, including acetic acid, propanoic acid, ethanol and methanol, were produced. In the case of methane conversion to acetic acid reported by Nizova et al. [4], the methyl group was derived from methane, whereas the carboxylic group was derived from CO_2. Spivey et al. [5] investigated the direct conversion of CO_2 and CH_4 over 5% Pt/carbon and 5% Pt/alumina catalyst. The formation of gaseous acetic acid at about 400 °C over 5% Pt/alumina catalyst was achieved. Generally speaking, the direct conversion of CO_2 and CH_4 to oxygenated compounds is not thermodynamically favorable [2], and efficient catalysts for economical and selective conversion have not been developed. Consequently, the development of novel and selective catalysts for direct conversion of CH_4 and CO_2 to highly valued products is still a challenging task to chemists worldwide.

Semiconductor catalysts have received considerable attention in recent years because of their photocatalytic activity for initiating redox reactions [6–8]. Conversion of CO_2 is a reduction reaction, while that of CH_4 is an oxygenation process. The process, which realizes the conversion of CH_4 and CO_2 at the same time, is an ideal redox reaction. Reports in the literature [9–12] revealed that

* Corresponding author. Tel.: +86 22 402976.
E-mail address: shzhong@public.tpt.tj.cn (S. Zhong).

0920-5861/$ – see front matter © 2004 Elsevier B.V. All rights reserved.
doi:10.1016/j.cattod.2004.09.004

some photocatalyst systems have the ability of efficient photoinduced reduction of CO_2 to formate, CO, and C_1–C_3 compounds, etc. In recent years, several groups reported the photocatalytic conversion of methane to methanol [13] and CO [14]. Using UV photo-energy to break the thermodynamic limitations of some thermodynamically unfavorable reactions have been proved to be effective [13,15]. We previously reported [14,16] the catalytic synthesis of methanol from CO_2 and H_2O and CH_4 and H_2O using UV-induced catalysis technology. Therefore, photocatalytic conversion of CH_4 and CO_2 together may be a promising method for direct conversion of CH_4 and CO_2 to oxygenated compounds. In this paper, we will report direct synthesis of oxygenates over the coupled semiconductor from gaseous CH_4 and CO_2 by UV induction at low temperature. In the present study, the coupled semiconductor catalyst of Cu/CdS–TiO_2/SiO_2 was prepared by the multi-step impregnation.

2. Experimental

2.1. Preparation of photocatalyst

Tetrabutyl titanate and cadmium perchlorate of reagent grade were purchased from Tianjin Reagent Factory. A variety of organic solvents of reagent grade were used after redistilled. Water was distilled twice under atmospheric pressure. Commercially available silica gel (Qingdao Ocean Chemical Factory) was used as the bulk material, which was in 20–40 mesh with a specific surface area of 364 m^2/g.

2.1.1. TiO_2/SiO_2

The TiO_2/SiO_2 were prepared by impregnation of the silica with an ethanol solution of tetrabutyl titanate for 2 h under reflux condition, as already reported in [17]. The filtrate was calcined for 4 h at 773 K. The loading of TiO_2 was adjusted to 15 wt.%.

2.1.2. CdS–TiO_2/SiO_2

TiO_2/SiO_2 was added into a solution of cadmium perchlorate and stirred for 2 h. The stoichiometric amount of H_2S was dropped in under vigorous shaking. Cl^- was washed off by a large amount of water. Heat treatment of the solid was carried out at 523 K for 4 h. The CdS loading was set at 5 wt.%.

2.1.3. Cu/CdS–TiO_2/SiO_2

Cu catalyst was prepared by the incipient wet impregnation using $Cu(NO_3)_2$ as the metal precursor. The solid was dried overnight in air at 373 K and calcined at 773 K in air for 4 h for complete decomposition of the precursor. The Cu loading was kept at 0.5 wt.%. Before the reaction, the catalyst was reduced at 563 K in a stream of 7% H_2–N_2 for at least 2 h.

2.2. Catalyst characterization

Samples were reduced in the temperature-programmed reduction (TPR) mode using a quartz U-shaped reactor by heating from room temperature to 1173 K at the heating rate of 8 K min^{-1}, in 7% (v/v) H_2 in N_2. The gas mixture flow rate was preset at 10 ml/min at atmospheric pressure. The sample weight was 20 mg.

The laser Raman spectra were obtained with a BRUKER RFS100/S spectrometer using the Nd: YAG laser as emission source and D-418-S detector. The output laser power was 530 mW. X-ray diffraction patterns were obtained by using a Rigaku Rint-2308 diffractometer with Ni-filtered Cu Kα irradiation. UV–vis diffuse reflectance spectra were recorded by a spectrophotometer (Perkin-Elmer, Lambda 35) using barium sulphate as reference sample. BET surface area was determined using N_2 as adsorbate at 77 K with a Quantachrom ChemBET 3000 apparatus.

The Infrared spectra of CO_2, CH_4 adsorbed on the catalysts and the bare catalysts were recorded on a Hitachi 270-30 spectrometer. The samples were pressed to tablets prior to the adsorption, placed in a steel holder and introduced into a copper cell with KBr windows. Then they were heated to 473 K in vacuum (10^{-5} Torr) for 2 h. CO_2 and CH_4 were adsorbed at 423 K under the pressure of 5–10 Torr for 2 h and evacuated for several minutes to 10^{-4} Torr.

2.3. Investigation of photocatalytic reaction

The photocatalytic reaction was carried out in a continuous flow quartz-fixed-bed reactor with a diameter of 35 mm. A 125 W ultrahigh pressure mercury lamp was used as the light source, as shown in Fig. 1. The pressure of reaction system was kept at 1 atm, and the temperature was not higher than 473 K. Ten grams of catalyst was loaded into the reactor and reduced again in situ at 563 K in the 7% H_2–N_2 flow for 2 h. The flow rate of the feed gases was controlled by mass flow meters. The temperature of the catalyst bed, measured by a chromel–alumel thermocouple,

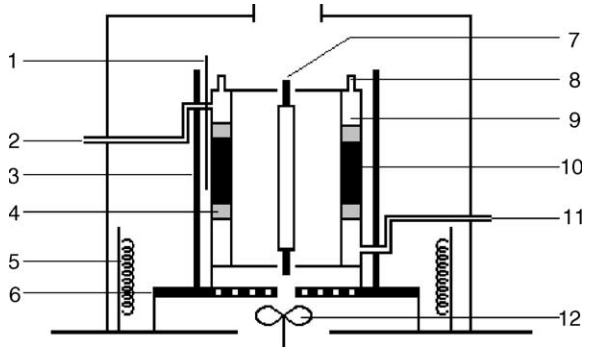

Fig. 1. Schematic representative of photocatalytic reaction system: (1) thermocouple; (2) gas outlet; (3) aluminum foil; (4) sieve plate; (5) heater; (6) graphite plate; (7) mercury lamp; (8) catalyst inlet; (9) quartz reactor; (10) catalyst bed; (11) gas inlet; (12) fan.

was kept constant within ±1 K. The composition of reactants/products mixture was analyzed with an on-line Agilent 4890D gas chromatograph equipped with a TCD detector.

3. Results and discussion

3.1. Catalyst structure

A quantitative comparison of the BET surface area of the silica support, TiO_2/SiO_2, $CdS–TiO_2/SiO_2$ and $Cu/CdS–TiO_2/SiO_2$ are given in Table 1. The photocatalyst retains a rather large surface area of 264 m^2/g after loading of TiO_2, CdS and Cu on the supporter. In general, it is well known that TiO_2 anatase particles possess the surface area below 100 m^2/g. Loading on SiO_2 remarkably increases the surface area of the coupled semiconductor catalyst, which may enhance CO_2 and CH_4 adsorption.

Fig. 2 presents TPR profiles of the samples studied. One can see two peaks over sample 1 at 246 and 268 °C. Peak at 246 °C is due to reduction of fine dispersed CuO and another peak at 268 °C indicates reduction of bigger particles [18]. The reduction peak of sample 2 reduces to 242 °C, which is evidence for that Ti^{4+} can lower the reduction temperature of CuO. There are two peaks of hydrogen consumption in the TPR profiles of sample 3 (344 and 488 °C) and sample 4 (286 and 451 °C). The first one is due to reduction of CuO and the second is for Cd^{2+}. The lower reduction temperature of CuO of sample 4 can be interpreted by that TiO_2 has strong interaction with Cu^{2+} and it changes the reduction route of CuO. The position of reduction peak of sample 4, resembling to sample 2, indicates that the chemical environment of CuO of samples 2 and 4 are homologous. In other words, CuO on sample 4 only spreads over anatase particles.

Fig. 3 shows UV–vis absorption spectra of CdS/SiO_2, TiO_2/SiO_2 and $CdS–TiO_2/SiO_2$. Since SiO_2 is transparent in the wavelength range between 250 and 800 nm, the spectra of CdS/SiO_2 and TiO_2/SiO_2 are very similar to that of bulk CdS and TiO_2, except for the blue shifts of the band gap due to the presence of smaller particles [19]. The shape of $CdS–TiO_2/SiO_2$ is a combination of those for CdS/SiO_2 and TiO_2/SiO_2, showing the absorption edges also around 510 and 370 nm. Accordingly, both $CdS–TiO_2/SiO_2$ and CdS/SiO_2 are yellow in color, for which fine particles of CdS dispersed on silica support should be responsible [20].

Fig. 4 shows IR spectra of silica support and semiconductor samples. Absorption signals assigned to

Table 1
BET surface area of catalysts

Sample	$S_{BET}(m^2/g)$
SiO_2	364
TiO_2/SiO_2	292
$CdS–TiO_2/SiO_2$	268
$Cu/CdS–TiO_2/SiO_2$	264

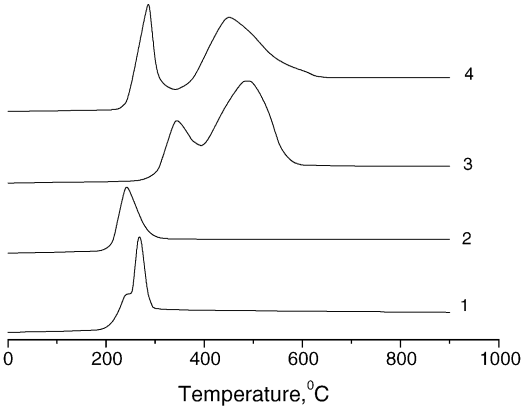

Fig. 2. TPR spectra of Cu-samples: (1) CuO/SiO_2; (2) $CuO/TiO_2/SiO_2$; (3) $CuO/CdS/SiO_2$; (4) $CuO/CdS–TiO_2/SiO_2$.

Si–O–Si vibrations are observed at about 1081 cm^{-1} (asymmetrical Si–O–Si valency vibrations), 800 cm^{-1} (symmetrical Si–O–Si valency vibrations of the silica skeleton) and 430 cm^{-1} (deformation vibrations of the silica skeleton) in all cases [21], while absorption bands at 1734 and 723 cm^{-1} in the spectra of CdS/SiO_2 are attributed to the surface dispersed CdS. Absorption peak at 962 cm^{-1} leads to conclusion on formation of the Ti–O–Si structure in TiO_2/SiO_2 [21]. The fact of the main silica band (1081 cm^{-1}) shifting to 1084 cm^{-1} (TiO_2/SiO_2) and 1086 cm^{-1} ($CdS–TiO_2/SiO_2$) also confirms that TiO_2 particles are chemically bound to the SiO_2 supports. The spectral feature for $Cu–CdS–TiO_2/SiO_2$ is almost the same as that for $CdS–TiO_2/SiO_2$. Bands at 1732 and 721 cm^{-1} are attributed to CdS, while 1351 and 964 cm^{-1} are due to TiO_2. Because of the low loading, the signals of copper are not observed in the case of IR.

In XRD patterns, it is clearly observed that CdS diffraction peak does not appear in the patterns of $Cu/CdS–TiO_2/SiO_2$. All the observed reflections can be attributed to anatase. This is a good indication of high dispersion of cadmium on silica supports. This is also

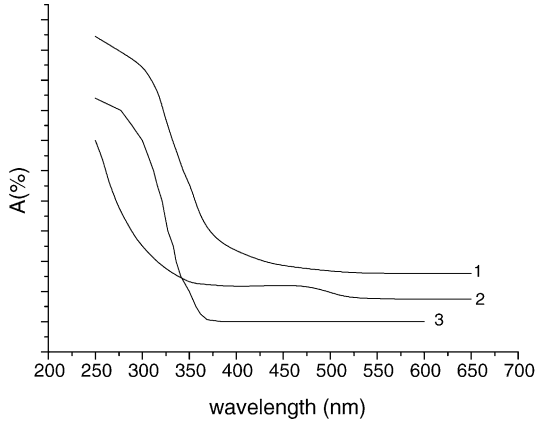

Fig. 3. UV–vis absorption spectra of CdS/SiO_2, TiO_2/SiO_2 and $CdS–TiO_2/SiO_2$: (1) CdS/SiO_2; (2) $CdS–TiO_2/SiO_2$; (3) TiO_2/SiO_2.

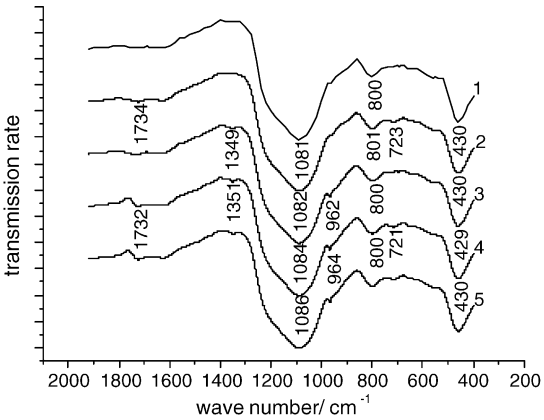

Fig. 4. IR spectra of silica support and semiconductor samples: (1) SiO_2; (2) CdS/SiO_2; (3) TiO_2/SiO_2; (4) $CdS–TiO_2/SiO_2$; (5) $Cu/CdS–TiO_2/SiO_2$.

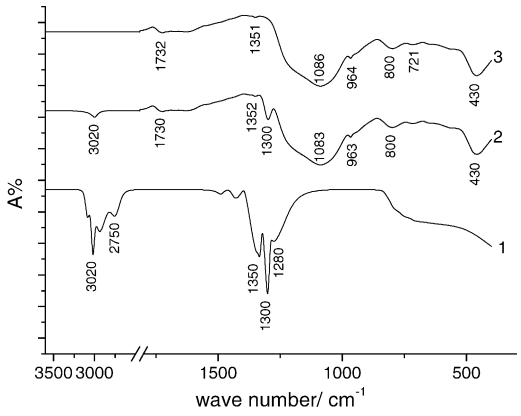

Fig. 6. IR spectra of CH_4 absorbed on $Cu/CdS–TiO_2/SiO_2$ sample at 373 K: (1) CH_4; (2) $Cu/CdS–TiO_2/SiO_2 + CH_4$ (ab); (3) $Cu/CdS–TiO_2/SiO_2$.

consistent with the result of Raman spectra. Fig. 5 shows Raman spectra of the $Cu/CdS–TiO_2/SiO_2$ sample. These Raman peaks at 642, 517, 402 and 151 cm^{-1} are due to anatase [22]. No peak denoting CdS and Cu is observed.

On the basis of above results, we can deduce a possible structure of $Cu/CdS–TiO_2/SiO_2$ catalyst as shown in Scheme 1. That is, the anatase particles are spread over surface of silica supporter by anchoring onto Si–O–Si structure with O^{2-} bridging. CdS grains are dispersed on layer of anatase. Cu seeds dotted over anatase particles.

3.2. Surface species

Figs. 6 and 7 show IR spectra of methane and carbon dioxide absorbed on $Cu/CdS–TiO_2/SiO_2$ sample, respectively. Methane absorbed on the coupled semiconductor formed two absorption bonds at 3020 and 1300 cm^{-1}, which indicate weak interaction between methane and coupled semiconductor [23]. CO_2 absorbed on the Cu-catalyst generates some surface species, as shown at 1389 and 1530 cm^{-1}, indicating the formation of surface formate species. 1311 cm^{-1} is attributed to bidentate and 1930 cm^{-1} is due to linear absorption of carbon dioxide on Cu metal. 2050 cm^{-1} indicates linear absorption species too [24].

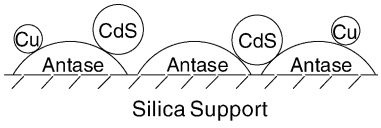

Scheme 1. Possible structure of $Cu/CdS–TiO_2/SiO_2$ catalyst.

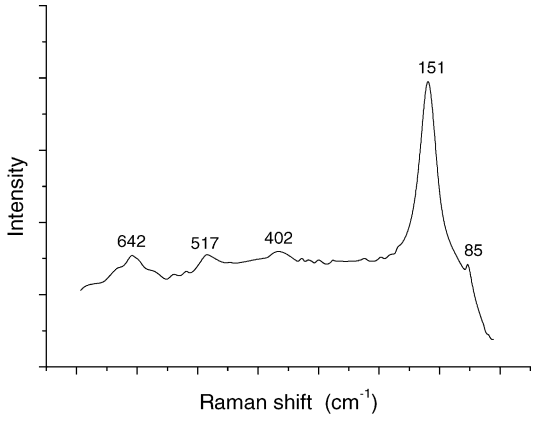

Fig. 5. Raman spectra of $Cu/CdS–TiO_2/SiO_2$ sample.

3.3. Catalytic activity of the Cu-catalyst

We have carried out the direct conversion of methane and carbon dioxide to oxygenated compounds over $Cu/CdS–TiO_2/SiO_2$ catalyst. Without UV radiation or photocatalyst, no conversions of methane and carbon dioxide are observed at all investigated temperatures. While UV light is on, conversion rates of CO_2 and CH_4 increase with the increase of temperature. The best selectivity of acetone was 92.3% at 120 °C. When the reaction temperature raises up to 200 °C, the conversion of CO_2 and CH_4 decreases dramatically because of the desorption of CO_2 and CH_4. Unfortunately, the conversion of CO_2 and CH_4 reduces to zero in about 2 h.

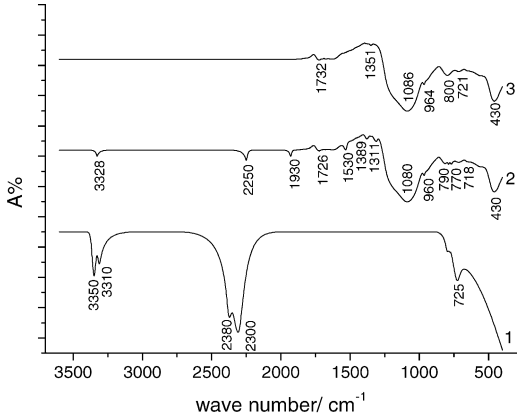

Fig. 7. IR spectra of CO_2 absorbed on $Cu/CdS–TiO_2/SiO_2$ sample at 373 K: (1) CO_2; (2) $Cu/CdS–TiO_2/SiO_2 + CO_2$ (ab); (3) $Cu/CdS–TiO_2/SiO_2$.

Table 2
Photocatalytic conversion methane and carbon dioxide over Cu/CdS–TiO_2/SiO_2

Temperature (°C)	Conversion (%)		Selectivity (%)			
	CO_2	CH_4	CH_3COOH	CH_3CH_3	CH_3COCH_3	CO
30	0	0	–	–	–	–
80	0.07	0.11	–	46.7	0	53.3
120	0.74	1.47	Trace	3.1	92.3	4.6
150	0.79	1.54	Trace	7.5	87.6	4.9

Reaction conditions: 1 atm; CO_2/CH_4 = 1/1 (molar ratio); UV intensity, 20.0 mW cm^{-2}; space velocity = 200 h^{-1}.

At the same time, the catalyst was decolorized. The reason for it is the photo-corrosion of CdS promoted by TiO_2 [19] (Table 2).

3.4. Reaction mechanism

From these results, photocatalytic synthesis of acetone over Cu/CdS–TiO_2/SiO_2 catalyst from gaseous CO_2 and CH_4 may occur with the reaction mechanisms as given by Reactions. (1)–(7). Electrons and holes are generated by irradiation on the coupled semiconductor (1). $^*CH_3$ is produced through oxidation of CH_4 by the valence band holes, and protons are simultaneously released (Reaction (2)). The conduction band electrons reduce CO_2 to the $^*CO_2^-$ anion radical (3):

$$\text{Couple semiconductor} \xrightarrow{h\nu} e^- + h^+ \quad (1)$$

Oxidation reaction

$$CH_4 + h^+ \rightarrow {}^\bullet CH_3 + H^+(ad) \quad (2)$$

Reduction reaction

$$CO_2 + e^- \rightarrow {}^\bullet CO_2^-(ad) \quad (3)$$

$$^\bullet CH_3 + {}^\bullet CH_3 \rightarrow CH_3CH_3 \quad (4)$$

$$CH_4 + {}^\bullet CO_2^-(ad) \rightarrow CH_3COO^-(ad) + {}^\bullet H \quad (5)$$

$$CO_2^-(ad) + H^+ + e^- \rightarrow CO + OH^-(ad) \quad (6)$$

$$^\bullet CO_2^-(ad) + {}^\bullet H \longrightarrow {}^{:}CO\ (ad) + OH^- \quad (7)$$

$$^{:}CO\ (ad) + 2\,{}^\bullet CH_3 \longrightarrow CH_3COCH_3 \quad (8)$$

Then two $^*CH_3$ couple to produce ethane (Eq. (4)). If the $^*CO_2^-$ anion radicals are attacked by gaseous methane, acetic acid is formed (Eq. (5)), while cleavage of the C–O bond of the $^*CO_2^-$ anion radicals results in the formation of carbon monoxide (Eq. (6)). The $^*CO_2^-$ anion radicals react with $^*H$ to produce $^{:}CO$ (Eq. (7)) and $^{:}CO$ reacts with two $^*CH_3$ to form acetone.

4. Conclusion

The photocatalyst Cu/CdS–TiO_2/SiO_2 are synthesized by a multi-step impregnation method. TiO_2 is spread over silica support in a form of anatase. CdS particles are highly dispersed over TiO_2/SiO_2. Cu seeds dot on anatase particles. Acetone can be directly synthesized from CO_2 and CH_4 over this photocatalyst. The conversion was 0.74% for CO_2 and 1.47% for CH_4 with the selectivity of acetone of 92.3%. The by-products are ethane and carbon monoxide with selectivities of 3.1 and 4.6%, respectively.

Acknowledgement

This work was financially supported by the Key Fundamental Research Project of Ministry of Science and Technology of China (2001CCA03600).

References

[1] Y. Fujiwara, Y. Taniguchi, K. Takaki, M. Kurioka, T. Jintoku, T. Kitamura, Stud. Surf. Catal. 107 (1997) 275.
[2] W. Huang, K.-C. Xie, J.-P. Wang, Z.-H. Gao, L.-H. Yin, Q.-M. Zhu, J. Catal. 201 (2001) 100.
[3] Y.P. Zhang, Y. Li, Y. Wang, C.J. Liu, B. Eliasson, Fuel Process. Technol. 83 (2003) 101.
[4] G.V. Nizova, G.B. Shul'pin, G. Suss-Fink, S. Stanislas, Chem. Commun. 1998 (1998) 1885.
[5] E.M. Wilcox, G.W. Roberts, J.J. Spivey, Catal. Today 88 (2003) 83.
[6] A. Henglein, Top. Curr. Chem. 143 (1988) 115.
[7] P.V. Kamat, Chem. Rev. 93 (1993) 267.
[8] A. Hagfeldt, M. Grätzel, Chem. Rev. 95 (1995) 49.
[9] P. Johne, H. Kisch, J. Photochem. Photobio. A: Chem. 111 (1997) 223.
[10] T.F. Xie, D.J. Wang, L.J. Zhu, T.J. Li, Y.J. Xu, Mater. Chem. Phys. 70 (2001) 103.
[11] B.J. Liu, T. Torimoto, H. Yoneyama, J. Photochem. Photobio. A: Chem. 113 (1998) 93.
[12] S. Ichikawa, R. Doi, Catal. Today 27 (1996) 271.
[13] C.E. Taylor, R.P. Noceti, Catal. Today 55 (2000) 259.
[14] S.Z. Chen, S.H. Zhong, X.F. Xiao, Chin. J. Catal. 24 (2003) 67.
[15] K. Wada, K. Yoshida, Y. Watanabe, J. Chem. Soc., Faraday Trans. 91 (1995) 1647.
[16] L.X. Shang, Ph.D. Dissertation, Tianjin University, China, 2003.
[17] L.X. Shang, S.H. Zhong, Chin. J. Catal. 25 (2004) 182.
[18] O.V. Komova, A.V. Simakov, V.A. Rogov, D.I. Kochubei, G.V. Odegova, V.V. Kriventsov, E.A. Paukshtis, V.A. Ushakov, N.N. Sazonova, T.A. Nikoro, J. Mol. Catal. A: Chem. 161 (2000) 191.
[19] L. Spanhel, H. Weller, A. Henglein, Am. Chem. Soc. 109 (1987) 6632.
[20] K.R. Gopidas, M. Bohorquez, P.V. Kamat, J. Phys. Chem. 94 (1990) 6435.
[21] X.T. Gao, I.E. Wachs, Catal. Today 51 (1999) 233.
[22] X. Gao, S.R. Bare, J.L.G. Fierro, M.A. Banares, I.E. Wachs, J. Phys. Chem. B 102 (1998) 5653.
[23] C. Li, Q. Xin, J. Phys. Chem. 96 (1992) 7714.
[24] A.A. Davydov, M.L. Shepotko, A.A. Budneva, Catal. Today 24 (1995) 225.